Post-flight Analysis of the Mars Science Laboratory Entry Aerothermal Environment and Thermal Protection System Response

Todd R. White[1]
ERC Inc., Moffett Field, CA 94035

Milad Mahzari[2]
Georgia Institute of Technology, Atlanta, GA, 30332

Deepak Bose[3]
NASA Ames Research Center, Moffett Field, CA 94035

Jose A. Santos[4]
Sierra Lobo, Inc., Moffett Field, CA 94035

The Mars Science Laboratory rover landed at Gale Crater on August 5th, 2012. The rover was protected from the extreme heating environments of Martian atmospheric entry by an ablative heatshield. This tiled Phenolic Impregnated Carbon Ablator heatshield was instrumented with a suite of sensors that monitored the in-depth ablator temperature response and the surface pressure at discrete locations. This paper presents a comparison of the flight data with post-entry analysis at the discrete sensor locations. From the flight data, we postulate that the heatshield experienced roughness-induced turbulent transition due to roughness elements around the heatshield tile and sensor plugs. We find that the analytical ablator material model performs well and can be used directly with the in-depth temperature data. Finally, we assess the performance of the ablation sensors, and predict the bondline temperature rise. The flight data from the instrumentation, along with the successful landing of the rover, confirms the performance of the heatshield and the conservative heatshield design and margins process.

I. Nomenclature

ARAD	Analog Resistance Ablation Detector
BET	Best Estimated Trajectory
CFD	Computational Fluid Dynamics
DPLR	Data Parallel Line Relaxation flow solver
FIAT	Fully Implicit Ablation and Thermal response program
IMU	Inertial Measurement Unit
MEADS	Mars Entry Atmospheric Data System
MEDLI	Mars Science Laboratory Entry Descent and Landing Instrumentation
MISP	MEDLI Integrated Sensor Plug
MSL	Mars Science Laboratory
PICA	Phenolic Impregnated Carbon Ablator
RTV	Room Temperature Vulcanizing

[1] Research Scientist, Aerothermodynamics Branch, AIAA Member.
[2] Graduate Research Assistant, Guggenheim School of Aerospace Engineering, AIAA Student Member.
[3] Senior Research Scientist, Aerothermodynamics Branch, AIAA Associate Fellow.
[4] Mechanical Engineer, Thermal Protection Materials and Systems Branch, AIAA Member.

TC	Thermocouple
TCR	Thermal coefficient of resistance
TGA	Thermogravimetric analysis
TPS	Thermal Protection System
Re_{kk}	Reynolds number based on roughness height
Re_{θ}	Reynolds number based on boundary layer momentum thickness
θ	Boundary layer momentum thickness
μ	Viscosity
k	Roughness height

II. Introduction

The Mars Science Laboratory (MSL) was the largest Mars entry vehicle to date; the vehicle had an entry mass of 3153 kg and the heatshield was 4.5 meters in diameter.[1] As such, the MSL Entry, Descent, and Landing (EDL) system required new solutions to enable a safe landing. MSL flew a guided lifting entry to achieve higher landing elevations and a more precise landing ellipse. The lifting entry, combined with the large heatshield size led to the MSL heatshield being designed to withstand turbulent heating throughout the entire entry heat pulse.[2,3] The MSL design values for heating and shear stresses were far greater than design values for Pathfinder or the Mars Exploration rovers.[4] The expectation of high turbulent heating led to a change in the forebody thermal protection system materials. All previous United States Mars landers had relied on the SLA-561V Super Lightweight Ablator material as the forebody heatshield; however, due to the high heating and shear conditions expected during MSL's turbulent entry, the MSL heatshield material was switched from SLA-561V to the Phenolic Impregnated Carbon Ablator (PICA).[5]

PICA had flight heritage on the Stardust re-entry capsule, whose monolithic heatshield successfully survived the highest heating environments of any NASA earth entry vehicle to date. The MSL 4.5 meter diameter made a monolithic single-piece heatshield of PICA impossible, however. At the time of the MSL's TPS switch, PICA was undergoing extensive characterization as a candidate heatshield material for NASA's Crew Exploration Vehicle (CEV). The CEV heatshield was even larger than MSL, and CEV's development activities enabled another solution for MSL: a tiled ablative TPS. The MSL PICA heatshield was comprised of a total of 113 tiles of 23 different shapes. The gaps between the tiles were filled with a silicone elastomer bonding agent that helped to relieve stresses due to differences in thermal expansion of the different tiles. Besides improvements in heatshield technology, MSL employed several other novel EDL approaches, including an enormous supersonically deployed parachute, and a skycrane final descent stage for a tethered soft-landing. All of these technologies enabled the successful landing of the Mars Science Laboratory *Curiosity* rover on August 5th, 2012.

The challenges of the MSL EDL system, as well as those of future Mars exploration inspired the extensive instrumentation of the MSL heatshield. The instrumentation focused on gathering data to characterize the hypersonic aerodynamics, aerothermodynamics, and heatshield performance. This valuable aerothermal environment and heatshield performance data were gathered by in-situ temperature and pressure measurements during the MSL entry. The system responsible for these measurements was the MSL Entry Descent and Landing Instrumentation (MEDLI) suite.[6,7] MEDLI consisted of two types of instrumentation. The first type was the MEDLI Instrumented Sensor Plug (MISP), which consisted of seven plugs that measured the ablator performance and the in-depth thermal response of the PICA heatshield. The second type of instrument was the Mars Entry Atmospheric Data System (MEADS), which used seven transducers to measure the surface pressure across the heatshield. Preliminary results and analysis from the MEADS[8] and MISP[9,10] systems were published in the months following the successful landing. This paper will focus on data returned from the MISP.

The location of the MISP instrumentation as installed on the MSL heatshield is shown in Fig. 1a. The plugs were numbered as follows: MISP1 and MISP4 were installed in the stagnation region, while MISP5 and MISP7 were embedded in the geometric apex region to capture maximum laminar heating. MISP2, MISP3, and MISP6 were located in the leeside forebody to capture turbulent heating levels, as this region was expected to experience maximum heat flux. The plugs were arranged along or near the line of symmetry to capture the development and progression of the boundary layer transition front. MISP2 and MISP3 were installed slightly away from the centerline.

The MISP consisted of a cylindrical plug of PICA (1.3" diameter and 1.14" deep) PICA cylindrical plugs, with embedded instruments, as shown in Fig. 1b. The MISP were installed on the heatshield using the RTV-560 silicone-elastomer bonding agent on the bottom and sides of the PICA cylinder.

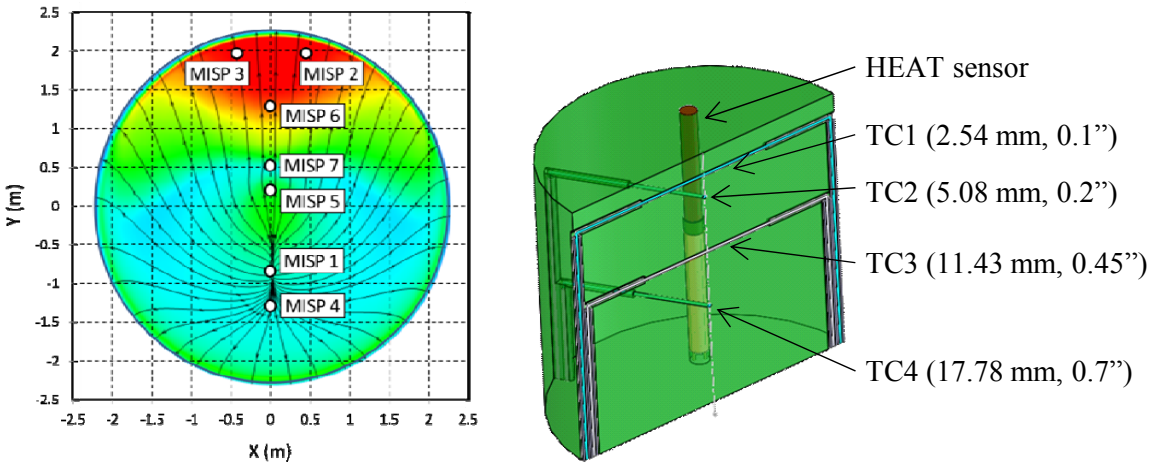

(a) Sensor locations (b) MISP cross section

Fig. 1 Locations of the MEDLI sensors and detail of MISP.

Each MISP plug contained four Type-K (chromel-alumel) TCs, each with a 0.012" wire diameter. The TCs were manufactured and installed according to the ASTM standard for low-conductivity materials.[10] The TCs were placed at nominal depths of 0.1, 0.2, 0.45, and 0.7 inch (2.54, 5.08, 11.43, and 17.78 mm) from the top surface. The top thermocouples were expected to be more responsive to changes in the surface heating conditions, while the deeper thermocouples were expected to measure in-depth thermal response as heat was conducted through the thickness of the recessing and pyrolyzing material. After installation, the measured depths of as-installed TCs were made using X-Ray. Table 1 details the TC depths for each MISP.

Table 1 X-Ray depths of thermocouples installed at each MISP location

Plug	TC1	TC2	TC3	TC4
	mm	*mm*	*mm*	*mm*
Design	*2.54*	*5.08*	*11.43*	*17.78*
MISP1	2.65	5.09	11.49	17.87
MISP2	2.68	5.16	11.57	17.77
MISP3	2.61	4.91	11.59	17.60
MISP4	2.47	5.39	11.32	17.94
MISP5	2.53	4.86		
MISP6	2.73	5.15	11.67	17.66
MISP7	2.39	4.89		

In addition to the thermocouples, each plug contained an ablation sensor, called the HEAT sensor (Hollow aErothermal Ablation and Temperature).[12] The HEAT sensor is a variant of the Analog Resistance Ablation Detector (ARAD) sensor, which was used to measure recession of the Galileo Jupiter probe's carbon phenolic heatshield.[13] Each HEAT consisted of two platinum-tungsten (Pt-W) wires wound around a tube made of Kapton a polyimide insulator. As each HEAT sensor was heated, the Kapton tube charred and became electrically conductive. The conductive path shorted the wires at the char front whose location can be detected by a resistance measurement. The response of each HEAT sensor was recorded as resistance (using measured voltage) versus time, which was then converted into a time-varying HEAT sensor depth, using the nearby TC data to correct for the resistivity of Pt-W wires. The HEAT sensors were sampled at 8 Hz, while the shallower TCs were sampled at 8 Hz, and deeper TCs were sampled at 1-2 Hz. Not all of the sensors were connected due to channel limitations, namely TC3 and TC4 at both MISP5 and MISP7, as well as the HEAT at MISP4. Table 2 summarizes the data rates for all the sensors in each MISP.

Table 2 Sampling rates for MISP

Plug	TC1 *Hz*	TC2 *Hz*	TC3 *Hz*	TC4 *Hz*	HEAT *Hz*
MISP1	8	8	1	1	8
MISP2	8	8	2	2	8
MISP3	8	8	1	1	8
MISP4	8	8	1	1	
MISP5	8	8			8
MISP6	8	8	1	1	8
MISP7	2	2			8

Blank entries indicate a sensor was not recorded due to a limited number of data channels

The complete MISP dataset was stored onboard the *Curiosity* rover during entry, and received a few days after landing. Channels of raw voltages and currents were converted into thermocouple temperatures and HEAT sensor resistances. All 24 MISP temperatures and 6 HEAT sensor resistances signals were received. All thermocouples returned data successfully, and the traces appeared to be virtually noise free. The data from the HEAT sensors, however, showed unusual behavior during the heat pulse. We show comparisons of some of the HEAT data with TC data and analysis tool results in Section IV. The as-received MISP temperatures are shown in Fig. 2. Red lines represent the shallowest thermocouple (TC1), green TC2, blue TC3, and brown TC4. All the TC1 data was returned and remained well below the 1370 °C upper temperature limit for a Type K TC, indicating with certainty that there was less than 2.54 mm of recession at all of the MISP locations.

Since each MISP measured in-depth temperatures and not surface heating, a material response model that relates surface aerothermal parameters to in-depth temperatures was needed. Such an inverse reconstruction (IR) attempts to estimate the surface heating by minimizing the difference between the material response model predictions and sensor measurements. An IR methodology was successfully developed specifically for MEDLI post flight analysis.[13] The technique was successfully applied in reconstruction of the Mars Pathfinder entry environment based on in-depth thermocouple measurements.[15] Edquist *et al*. have used the MISP data and made qualitative comparisons with the IR inferred heating profiles.[16] The authors have previously noted the discernible slope change at TC1 indicating turbulent transition at MISP2, MISP3, MISP5, MISP6 and MISP7, and have used this data to infer transition time at these locations.[10]

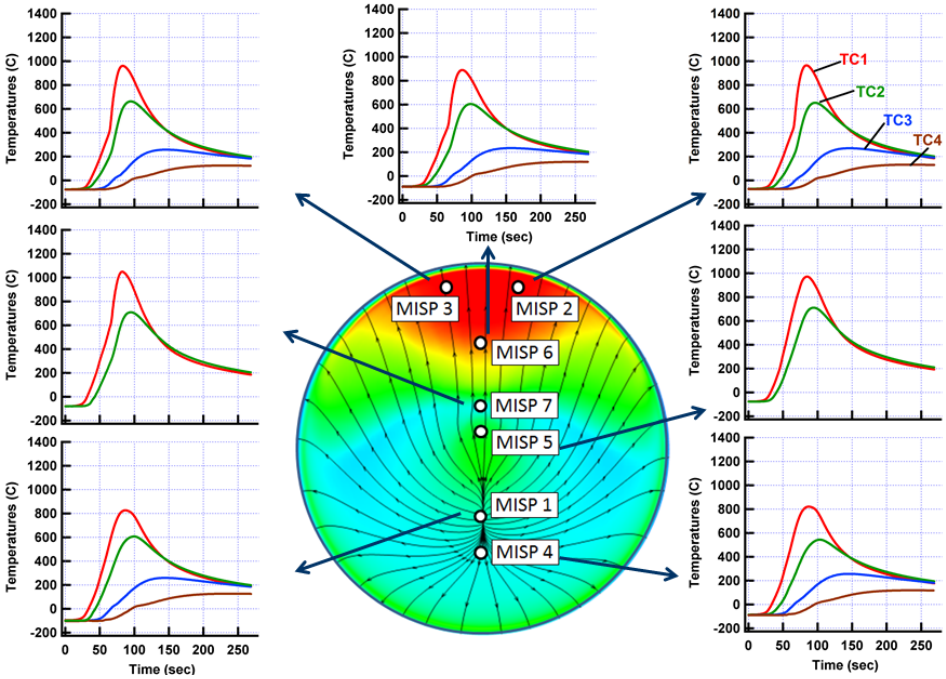

Fig. 2 MISP thermocouple data obtained during MSL entry. TC1, TC2, TC3, and TC4 represent readings of thermocouples at depths shown in Table 2.

This paper investigates heatshield performance using a combination of the MISP flight data and numerical models. First, in Section III, we examine the possible causes of turbulent transition in flight. To do so, we will examine several transition criteria, and identify the several causes of roughness associated with the MSL PICA heatshield. We use those heights along with flow field calculations to determine if roughness may have caused transition at the MISP locations. In Section IV and beyond, we focus on the in-depth temperature response of the TPS. We will use the flight TC data to anchor material response simulations. This anchoring will force our simulations to use the exact thermocouple response from flight, which we can use to evaluate the in-depth conduction calculation accuracy of our PICA ablator model. We use this anchoring process to evaluate how consistently we predict the other thermocouples traces and also to compare the thermocouples, ablator model, and HEAT sensor outputs together for consistency. In Section V, we calculate the bondline temperature rise at each of the MISP locations and determine an un-margined PICA thickness for the as-flown MSL trajectory.

III. Roughness-induced Transition at MISP Locations

The MSL heatshield was designed to withstand fully turbulent heating for the entire heat pulse. Traditionally, heatshield designers have used boundary layer Reynolds number-based correlations to assess when the flow will become turbulent. The most common, a smooth-wall transition criterion, is based on the momentum thickness Reynolds number, or Re_θ:

$$Re_\theta = \rho_e u_e \theta / \mu_e$$

Re_θ is the Reynolds number calculated using boundary layer edge values of density (ρ), viscosity (μ), and velocity (u), with a length scale determined by the momentum thickness, θ. For MSL design, a simple Re_θ criterion was considered: turbulent environments would be used as soon as any location on the heatshield experienced a Re_θ value greater than 200. Since this was predicted to happen very early on, the heatshield was sized for fully turbulent heating at all times to simplify the design process.

To assess the smooth wall transition criteria, we must employ flow field calculations. For this work, these calculations are performed with the DPLR non-equilibrium Navier-Stokes computational fluid dynamics (CFD) solver.[17] The solutions are performed along the Best Estimated Trajectory (BET) incorporating MEADS and Inertial Measurement Unit (IMU) flight data.[18] The flow around the heatshield is modeled as thermochemical non-equilibrium flow using the Mitcheltree and Gnoffo 8-species (CO_2, CO, N_2, O_2, NO, C, N, and O) 12-reaction Mars model.[19] The Martian atmosphere is modeled as 97% CO_2 and 3% N_2 by mass, and the TPS surface is treated as an unblown non-slip radiative equilibrium wall with constant emissivity ($\varepsilon = 0.89$) and the Mitcheltree/Gnoffo surface catalycity model.

Using these CFD calculations, we can extract the value of Re_θ at each MISP location. The authors have previously presented the inferred transition times based on MISP data, and also observed that the MISP transition times did not follow the smooth wall Re_θ criterion of 200 using an earlier estimated trajectory.[10] Table 3 includes the updated values of Re_θ on the BET, and we find that these earlier observations are still valid. The Re_θ criterion of 200 (as considered for MSL design) was conservative; the Re_θ values at MISP2 and MISP3 exceeded 200 more than 10 seconds *before* transition was observed at any of the MISP locations.

Table 3 Boundary layer transition times from MISP data compared to Re_θ predictions

Plug	Inferred transition Time	Predicted Transition Time with $Re_\theta > 200$	Calculated Re_θ at inferred transition time
	seconds	seconds	-
MISP3	63	52	394
MISP2	64	52	405
MISP6	65	57	293
MISP7	65	70	158
MISP5	73	No transition	125

Interestingly, the time for the transition front to progress from MISP2 and MISP3 to MISP7 was about two seconds (63 – 65 seconds) in flight. No Re_θ smooth wall criterion could reproduce this rapid front movement; the calculated Re_θ = 200 criterion predicts 18 seconds for the same progression. Figure 3 shows the temporal progression at each MISP and the spatial progression (at 65 seconds) of the momentum thickness Reynolds number on the MSL heatshield. There are a wide range of Re_θ values at the MISP at time of transition, making it difficult to deduce a better choice of a single Re_θ value as a transition criterion, or to explain the rapid progression of the transition front.

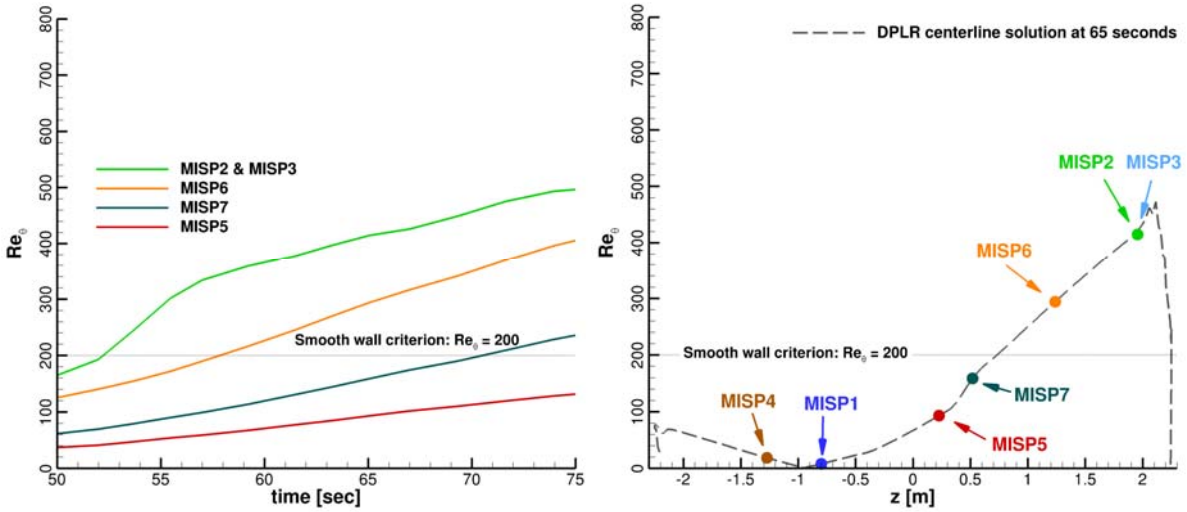

Fig. 3 Calculated momentum thickness Reynolds number at MISP locations.

The authors showed, in a preliminary analysis, that using a roughness based Reynolds number criteria might better explain the onset of turbulence and the rapid progression of the transition front. As locations on the heatshield were expected to exceed the MSL Re_θ criterion early on, the MSL heatshield designers did not consider roughness-induced turbulent transition criteria. Nonetheless, the MEDLI dataset provide a valuable opportunity to investigate their validity.

Roughness-induced transition criteria

The boundary layer Reynolds number used to evaluate roughness-induced transition is Re_{kk}, called the roughness Reynolds number. It is evaluated at a given roughness height, k, with the viscosity evaluated at the wall, according to:

$$Re_{kk} = \rho_k u_k \theta / \mu_w$$

There are generally two classes of roughness transition criteria: isolated roughness elements, and distributed roughness elements. Isolated roughness criteria correspond to transition because of a single element of known height acting as a trip, and whereas distributed roughness criteria are for a series of repeated roughness elements at a known height. Not surprisingly, the critical value of Re_{kk} above which the flow is tripped from laminar to turbulent flow (called transition criterion) are lower for distributed roughness than for isolated roughness.

The majority of literature on Re_{kk} criteria is based on experiments in air. Reda *et al.* provided transition criteria for both isolated (single element) and distributed elements (many smaller roughness elements) based on free-flight hemispherical models in the ballistic range.[20] The authors confirmed that for a given height, a distributed roughness was more effective than a single trip. For isolated roughness in air, the critical range of Re_{kk} values is 750 – 850, and for distributed roughness it is 250 ± 20%; based on these numbers, the ratio of critical Re_{kk} of isolated to distributed roughness is roughly 1/3. In another set of experiments, Reda *et al.* studied transition for isolated roughness elements in both air and CO_2. The authors reported that an isolated trip in CO_2 was more effective than air. For CO_2, the isolated roughness criterion is 600-800, or a reduction from the air criterion of ~1.3.[21] Unfortunately, there has been no experimental data or criterion published on distributed roughness in CO_2. For this study, we estimate a distributed roughness critical transition criterion for CO_2—we reduce the critical Re_{kk} for air by a factor of 1.3, to 190 ± 20%. Table 4 summarizes the roughness Reynolds number transition criteria.

Table 4 Roughness Reynolds number transition criteria

Roughness-induced transition criterion	Re_{kk} Range
Isolated roughness in air	750 - 850
Isolated roughness in CO_2	600 - 800
Distributed roughness in air	250 ± 20%
Distributed roughness in CO_2	190 ± 20%

Like the previous calculations of Re_θ, Re_{kk} must also be evaluated using CFD. Unlike Re_θ, however, there is an additional choice of roughness height (k) that strongly affects the value or Re_{kk}. For representative roughness heights, we revisit the assumptions used for MSL design, as well as some more recent characterizations of PICA roughness. We have identified three possible roughness elements that may have developed during entry and induced turbulent transition.

PICA Distributed Roughness

The first type of roughness is the roughness of ablated PICA. The first source of data is from the MSL heatshield design. In that analysis, a worst-case height of 0.6 mm was used, based on laser scans models tested in arc jet facilities.[2] The 0.6 mm roughness height came from turbulent wedge shear testing that was designed to envelope the entire MSL design environment, at heat rates at or above 200 W/cm^2. The MSL design also used this same height (k = 0.6 mm) for turbulent heating augmentation due to roughness.[16]

After landing, the MEDLI project conducted arc jet tests designed to simulate the MSL entry on coupons installed with MISPs.[9] Optical profilometry of the surrounding PICA on post-test samples, as shown in Fig. 4, yielded a considerably lower roughness height of k = 0.2 mm. This lower roughness height was for PICA samples arc jet tested at laminar conditions in the panel test facility, at cold wall heat rates of 45 W/cm^2. The authors believe the 0.2 mm roughness height is more representative of what probably occurred in flight.

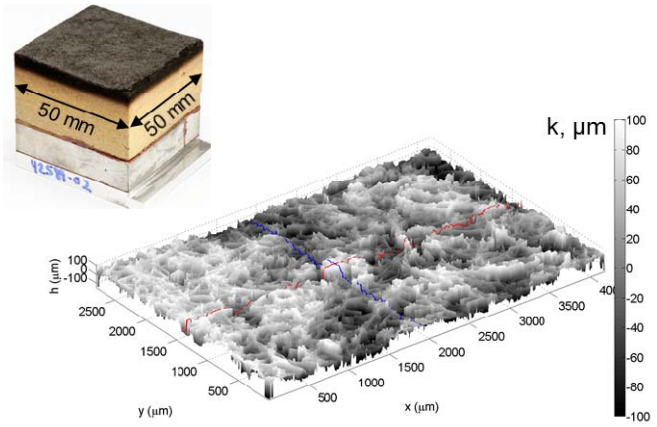

Fig. 4 Optical profilometry of PICA sample tested in arc jet

MISP Protuberance Roughness

The next source of possible roughness is from the instrumentation itself. To install each MISP to the heatshield, the sides of each MISP cylinder was coated with wet (uncured) RTV-560. This bonding agent can develop into a trip under certain conditions. This can happen in two ways: first, the exposed regions of the RTV may melt and swell to the surface, expanding from the original flush position. Second, at lower heating conditions, differential recession rates of the PICA and RTV-560 can lead to the RTV protruding around the edges of the PICA tiles.

This behavior yields a ridge that appears ring-like in shape and the resulting shape is sometimes referred to as a "caldera" or "fence"; these features have been observed over a wide range of arc jet tests. Figure 5 depicts a family of arc jet tested models, where the conditions range from 85 to 270 W/cm^2, where some models clearly exhibit the caldera effect. The caldera appears to be most prominent at lower heating-rate conditions (>100 W/cm^2) and is present in both stagnation and shear flow tests.

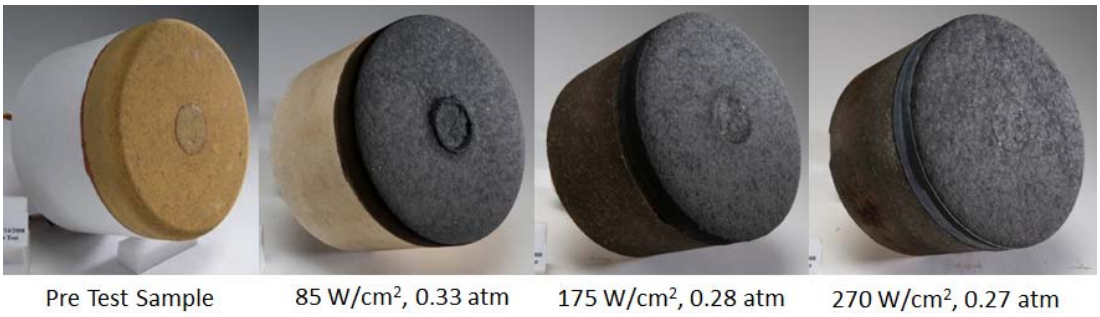

Fig. 5 RTV fencing on post-test MISP arc jet coupons

Figure 6(a) below shows a laser scan across one of the calderas developed in a low heating-rate (15 W/cm^2) shear flow test. Figure 6(b) and 6(c) show the trend of roughness heights as a function of both heat rate and arc jet test exposure time. More detail of these measurements and the arc jet conditions are presented in other publications but we do observe a strong correlation with height and test exposure time.[22] From this data, we infer the maximum RTV height of around 2 mm. The effect of a single isolated height may be compounded to act as more of a distributed roughness; there are seven plugs, and at each, the caldera could behave as two separate trips with a front and back fence. For centerline MISP locations (MISP1, MISP4, MISP5, MISP6 and MISP7) flow also passes over MEADS ports, but the MEADS are cavities rather than trips, and we do not expect these cavities to be as effective trips as the calderas formed at the MISPs.

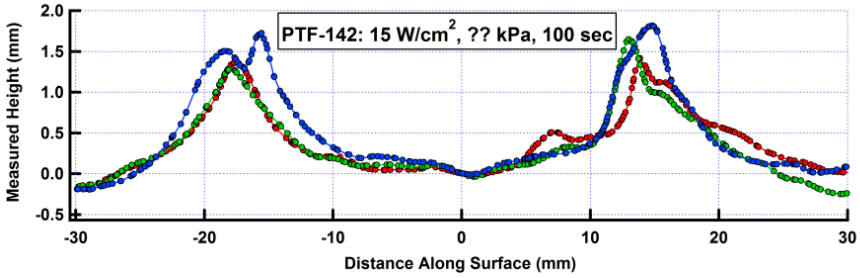

(a) Laser scan profiles showing fence height in post arc jet tested sample

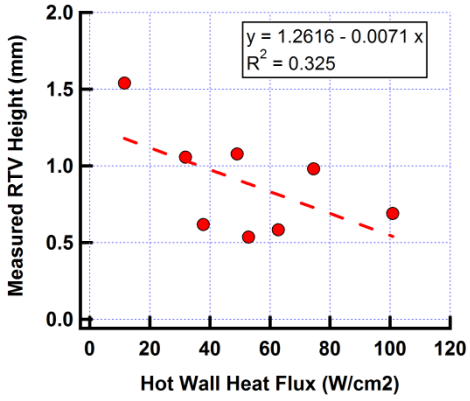

(b) Peak height as function of heat rate

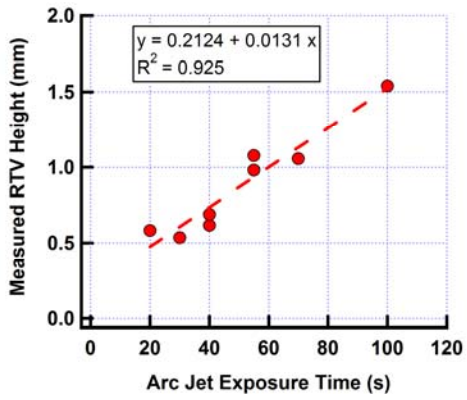

(c) Peak height as function of exposure time

Fig. 6 Measured peak roughness heights from MISP arc jet tests.[10]

MSL Tile Layout Roughness

The third possible source of roughness elements comes from the interfaces between the individual PICA tiles. As previously mentioned, the gaps between the PICA tiles were filled with the RTV-560 bonding agent that helped to relieve stresses due to differences and also to prevent hot gases from flowing between the tiles. Much like the MISP fences, the RTV may develop into a trip by swelling, melting, or differential recession. Figure 7 shows the tile

layout with MEDLI sensors (MISP are denoted T1 – T7) and streamlines from CFD. In the case of MISP2 and MISP3, a streamline may cross up to 10 tile gaps before reaching the plugs. The other MISPs that experienced turbulence (MISP5, MISP6, and MISP7) may have been affected by two to five tile gaps.

The MSL heatshield design team studied tile gap swelling and differential recession during arc jet tests, and noted gap heights of 2.0 up to 10 mm.[23] The current authors believe the 10 mm height is not applicable, as such heights developed only during severe over-test. In particular, those arc jet tests had very long test durations times and turbulent heating. We postulate that a height of around 2.0 mm height is more representative of flight. It is similar to the height of the caldera that can develop at the RTV around each MISP.

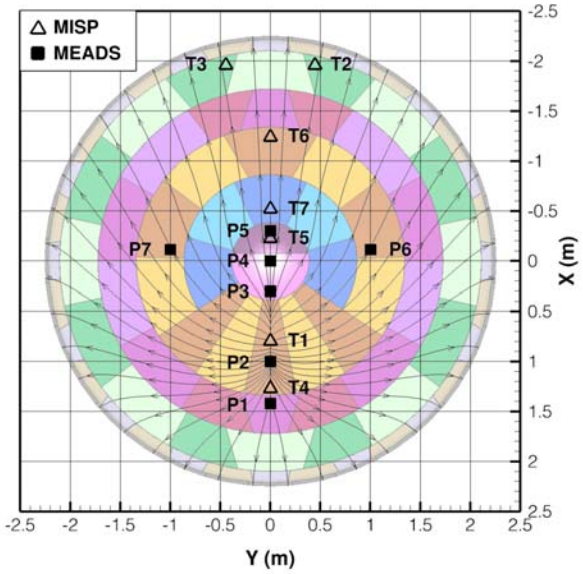

Fig. 7 MEDLI heatshield sensor locations with predicted streamlines.[16]

Table 5 summarizes the range of roughness heights from each of the possible roughness sources. We use these roughness heights and the DPLR results to estimate the values of Re_{kk}. As we did with momentum thickness Reynolds number, we will examine both the spatial and temporal variation of the roughness Reynolds number. Figure 8 shows Re_{kk} using the maximum distributed PICA roughness of 0.6 mm. We observe that the values of Re_{kk} with k = 0.6 mm are well below our estimated distributed roughness criterion; using the laminar PICA roughness height of 0.2 mm (not shown) yields even lower values of Re_{kk} everywhere. We conclude that PICA distributed roughness was unlikely to be the cause of transition for MSL.

Table 5 Distributed roughness heights on the MSL heatshield

Description	Height *mm*	Number or type
Distributed PICA roughness	0.2 – 0.6*	Distributed
Protrusions from MISP instrumentation	0.6 – 2.0	1 – 7
Protrusions from gap fillers between PICA tiles	2.0 – 10.0*	2 – 10

** Design values intended to capture worst-case behavior*

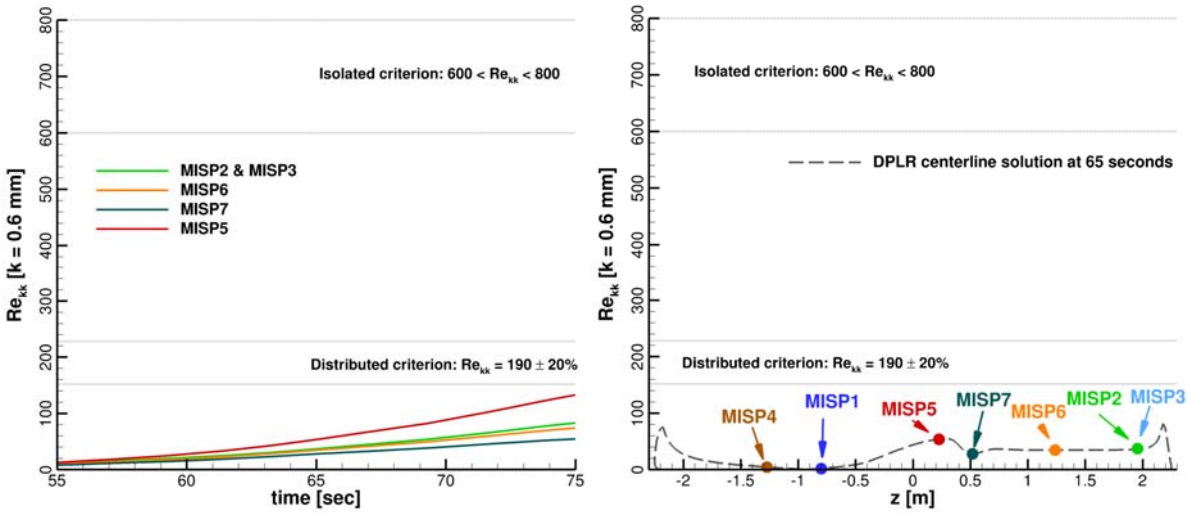

Fig. 8 Calculated distributed-roughness at MISP locations for roughness height of 0.6 mm.

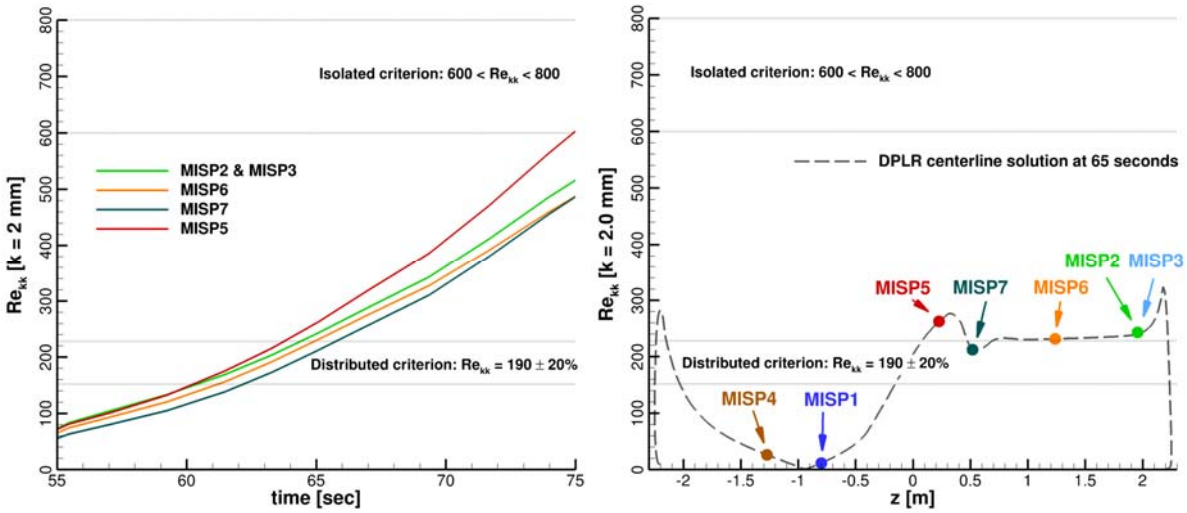

Fig. 9 Calculated distributed-roughness at MISP locations for roughness height of 2.0 mm.

We next investigate a roughness height of 2 mm, which represents the maximum roughness height observed from the MISP caldera, and also a roughness height observed in MSL testing of PICA tile gaps. Figure 9 shows better agreement with our CO_2 distributed criterion range of Re_{kk} = 190 ± 20%, though the spatial distribution indicates some of the Re_{kk} values at 65 seconds are above this range. Table 6 lists the transition times predicted with k = 2mm and the Re_{kk} CO_2 distributed roughness criterion. We see that the initial transition time is much closer to that inferred from flight data (62 to 63 seconds), and the speed of the transition front movement from MISP3 to MISP7 also matches much better. Table 6 also lists the calculated Re_{kk} value at the inferred transition time—for MISP2, MISP3, MISP6, and MISP7, we see the values of Re_{kk} fall around the upper end of our transition range for this height. The late transition time of MISP5 is still not well predicted, of all the plugs that experienced turbulent transition, MISP5 had the shortest running length from the stagnation point, and is therefore the least likely to be influenced by a series of upstream trips.

Table 6 Boundary layer transition times from MISP data compared to Re_{kk} predictions, k = 2mm

Plug	Inferred transition Time	Predicted Transition Time with Re_{kk} = 190	Calculated Re_{kk} at inferred transition time
	seconds	*seconds*	-
MISP3	63	62	198
MISP2	64	62	219
MISP6	65	63	230
MISP7	65	65	211
MISP5	73	62	525

In summary, using the MISP data, CFD results on the BET, and ground tests observations, we find that the rapid progression of the turbulent transition front was not well predicted by existing smooth wall Re_θ criteria. The observed transition may be explained through roughness induced transition. We have shown that transition was unlikely to be caused by PICA micro-scale roughness (0.6 mm or smaller), and that transition could have been induced by a series of 2 mm roughness elements caused by a combination of PICA gap fillers and/or MISP fences. Such behavior is consistent with our observations of RTV roughness heights and with roughness-induced transition criteria for CO_2. Additional ballistic range testing in CO_2 of models with distributed roughness could lead to better transition criterion to use for MSL. Such experiments would be applicable to future missions to planets with CO_2 dominated atmospheres (both Mars and Venus).

Ultimately, we may never learn what roughness elements developed on the MSL heatshield during entry. If *Curiosity* were to visit the heatshield it might be able to perform an examination. Such a detour is unlikely in the near future given the other scientific goals of the mission, but there is a precedent. In 2004, the *Opportunity* rover went to its heatshield crash site specifically to inspect the remains of the EDL hardware. Photographs of the TPS cross-sections, combined with reconstructed trajectories, allowed for some qualitative comparisons with the in-depth TPS response.[24] For the MSL heatshield, the MISP data provides us with much more direct measurements to examine the in-depth TPS response. It is to that subject that we now turn.

IV. In-depth Modeling of PICA Response Using MISP Flight Data

One method of analyzing the in-depth heatshield response with the MISP data is to solve just the in-depth heat conduction in the plug, using a TC as a temperature boundary condition in time. This is commonly known as a "TC driver" method. In each plug there are up to four thermocouples that can be used as a possible boundary condition to simulate the thermal response. For instance, the flight values from TC1 can be used to anchor the simulations, and comparisons made between all deeper TC flight values and model-predicted values. We expect that if we wish to focus primarily on our model validity for un-charred (virgin) PICA, we can use TC1 as a driver and compare to TC2. Alternatively, a deeper TC (such as TC3) may be used as a driver to compare TC4. In this way, the impact of virgin vs. char properties in the PICA model may be assessed independently.

One major advantage of the TC driver method is that it effectively decouples the in-depth heat conduction from the surface heating conditions. Thus, we focus on the performance of the in-depth material model without being affected by the uncertainty of surface heating. TC driver analysis can also be used to in developing a new material model or refining an existing one. Mahzari *et al.* make use of TC driver calculations to attempt to refine the PICA material response model using the MISP data and inverse techniques.[25]

To perform TC driver analysis, we will employ the same code and model used to design the size the MSL heatshield thickness. The code is the Fully Implicit Ablation and Thermal response (FIAT) material response program[26] with the v3.3 PICA model.[27] FIAT is an implicit ablation and thermal response solver for simulation of one-dimensional transient thermal energy transport in a multilayer stack of isotropic materials that can ablate from a front surface and decompose in-depth. The first step to performing TC driver calculations is to define the stack of TPS and substructure. While the MSL heatshield PICA thickness was uniform, the substructure stack varied depending on the location of the plug. Those locations were "Nose Cylindrical", "Flank", and "Outer Flank." Table 7 details the material stack of each MISP in these three zones. The most important differences between the regions are in the substructure. MISP2 and MISP3 on the outer flank have considerably thicker facesheets and a denser

aluminum honeycomb. These differences will not affect the shallower thermocouples, but they are important for bondline temperature response and TPS sizing discussed later in Section IV.

Table 7 Material and thicknesses of each MISP

Material	Thickness *mm*	Thickness *in*
Nose Cylindrical: MISP1, 5, & 7		
PICA	28.96	1.140
RTV bonding agent	0.25	0.010
PICA	2.54	0.100
Epoxy adhesive	0.30	0.012
Carbon facesheets	0.51	0.020
Aluminum honeycomb	63.50	2.500
Carbon facesheets	0.51	0.020
Flank: MISP4 & 6		
PICA	28.96	1.140
RTV bonding agent	0.25	0.010
PICA	2.54	0.100
Epoxy adhesive	0.30	0.012
Carbon facesheets	1.02	0.040
Aluminum honeycomb	63.50	2.500
Carbon facesheets	1.02	0.040
Outer Flank: MISP2 & 3		
PICA	28.96	1.140
RTV bonding agent	0.25	0.010
PICA	2.54	0.100
Epoxy adhesive	0.30	0.012
Carbon facesheets	2.54	0.100
Aluminum Honeycomb (2x density)	63.50	2.500
Carbon facesheets	2.54	0.100

We calculate the entire temperature field, as a function of time, using TC1 as the anchoring, or driver TC. We focus on MISP1 and MISP2 as they are representative of overall MISP performance (MISP1 experienced fully laminar heating, MISP2 experienced turbulent heating). Additionally, we have data for all four TCs in both MISP1 and MISP2. Before making quantitative comparisons, we examine contour plots of the in-depth temperature from TC1. Figure 10 shows the depth of each of the four thermocouples (dashed lines), as well as the approximate boundaries of the fully-charred, pyrolysis, and virgin PICA regions. For MISP1 and MISP2, TC1 and TC2 will be strongly influenced by the char properties of PICA in our FIAT model. That time occurs once the dashed TC line intersects the pyrolysis front line. TC3 and TC4, however, remain almost completely in the virgin zone. While the temperature response depends on the heat conduction from above, the simulated response from these thermocouples will be dominated by the virgin properties of PICA.

Based on the temperature field, it is clear that after 80 seconds, the top of the plug begins to cool. The temperature within the material continues to rise as the heat stored internally conducts up towards the surface, and down towards the substructure. An inflection in the MISP2 temperature field caused by turbulent transition is observed close to the surface. Deeper in the material it is difficult to discern the effect of turbulent transition.

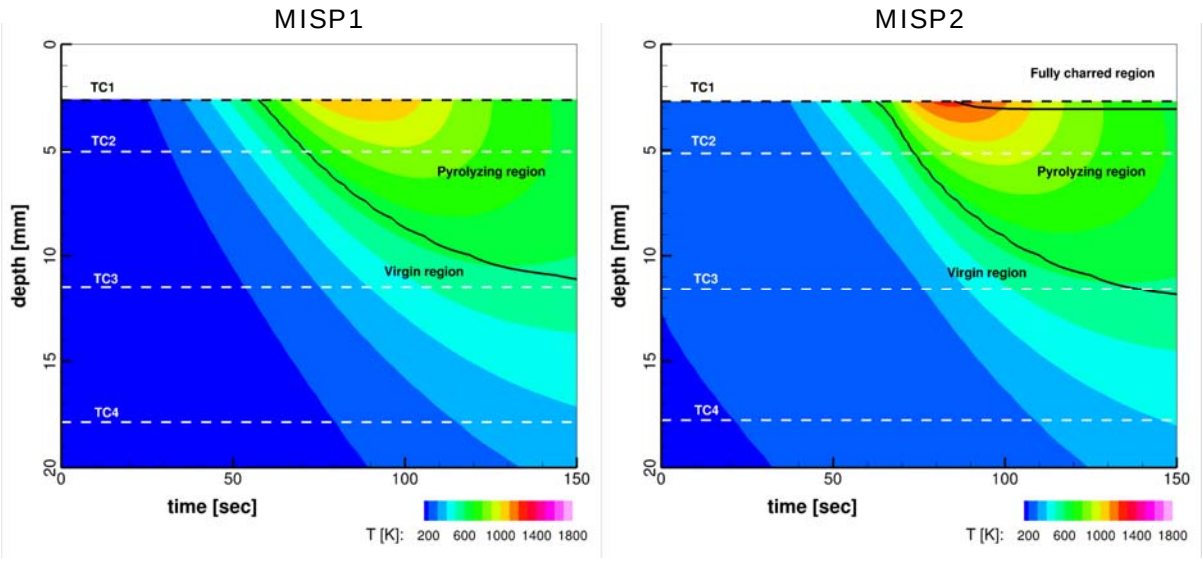

Fig. 10 MISP TC driver temperature field results using TC1.

We now proceed to comparing the flight thermocouple traces to those from TC driver simulations. Figure 11 shows the flight TC and FIAT TC driver simulated TC data together for the stagnation region plug, MISP1, and the lee-side shoulder plug, MISP2. To simplify the visual comparison, we are showing the temperature rise, calculated as:

$$\text{Temperature rise} = TC - TC_{t=0}$$

The dashed lines are the in-depth temperature predictions using the shallowest thermocouple data (TC1) directly from flight. We expect that the match between simulated and flight TC2 to be very good for two reasons. First, TC1 and TC2 are quite close (nominally 2.54 mm). As we saw above in the temperature fields, both TC1 and TC2 are in partially or fully developed char, and will be strongly influenced by PICA char properties. The agreement at TC2 is excellent. For MISP1, the peak of the simulated data is slightly lower than that of the flight data at 100 seconds, while for MISP2 the peak is slightly over-predicted at 92 seconds.

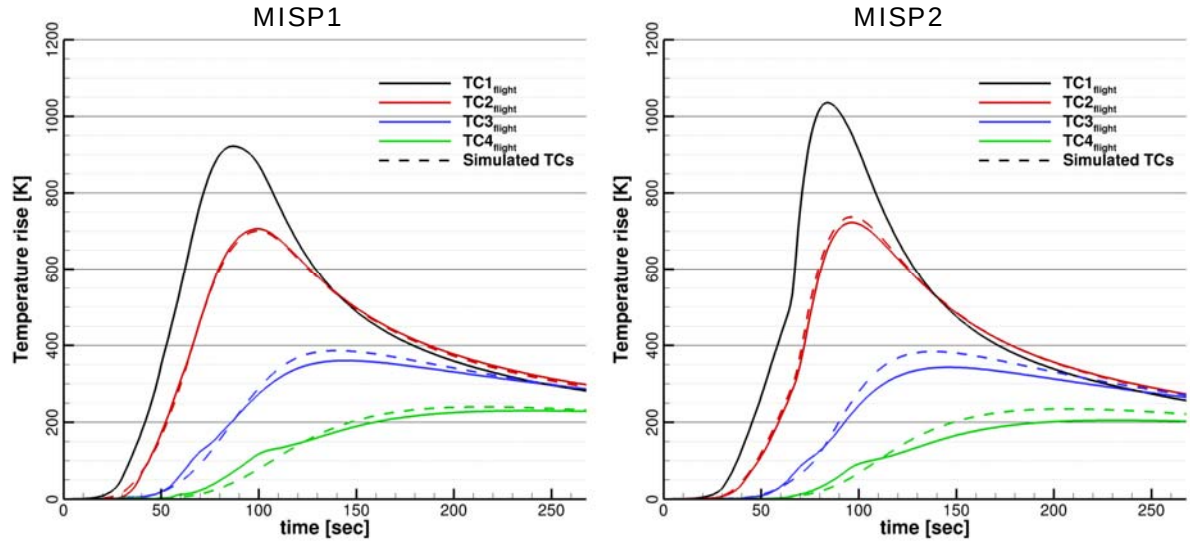

Fig. 11 Comparison of flight TC temperature rises with TC driver simulations.

Figure 12 shows the difference between the flight and simulated TC2 data. For MISP1, the predictions are within ±15 K. For MISP2, the FIAT model over-predicts by as much as 33 K. For both plugs, there is a slight under-

prediction in the temperatures during the cool down-period (t > 150 sec). For the deepest thermocouple, we use the three shallower thermocouples (TC1, TC2, and TC3) to drive the thermal response. In so doing, we can observe how well the model performs by comparing the flight and simulated TC response. We find that accumulated error increases with the increasing distance between the driver TC and TC4. The green line, for simulations using TC3 flight data, shows the best agreement. We can clearly observe the "hump" in flight data at 80 – 120 seconds, where the flight data are under-predicted at both plugs by all TC data by as much as 40 K. Unlike Fig. 12, there is an over-prediction in temperature during the cool down-period (t > 150 sec), except at MISP1. However, the FIAT model consistently over-predicts the peak temperature for TC4 experienced later in time (t = 200 sec).

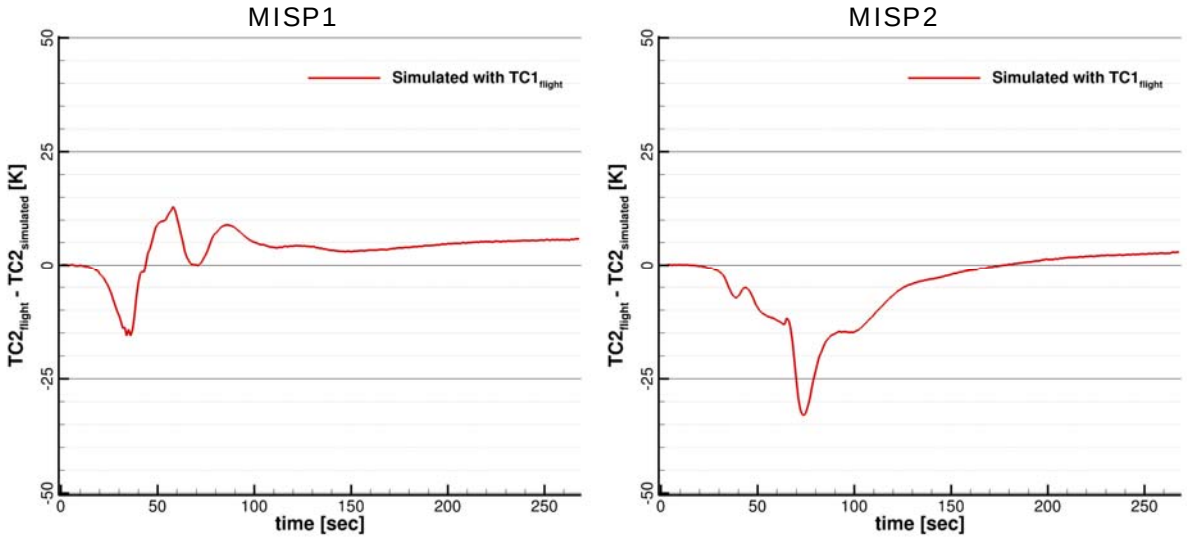

Fig. 12 Assessment of char in-depth model accuracy using flight data.

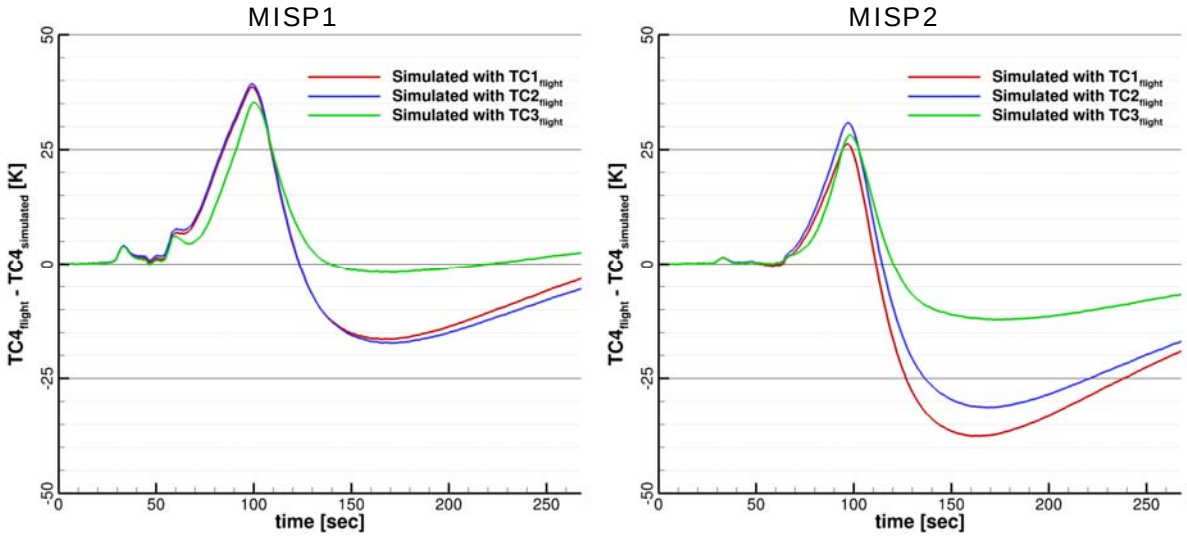

Fig. 13 Assessment of virgin in-depth model accuracy using flight data.

In summary, the in-depth FIAT model predicts the temperature response in flight quite well for all combinations of TC driver calculations, to well within ±50 K. Not surprisingly, the error grows as the TC being compared moves further away from the driver TC. Thus far we have relied solely on the thermocouple data to understand the MSL aerothermal environment and in-depth ablator response. However, six of the seven MISPs returned data from HEAT ablation sensors.[12] The raw HEAT data is a resistance measurement as a function of time, and this resistance measurement is proportional to some depth within the plug itself. If there are very high recession rates, the HEAT

sensor actually tracks the recession front. However, in the MSL heating environment, the depth reported by the HEAT sensor is harder to interpret. More details on the calibration of the HEAT using ground test has been published, and we use the ground test data from calibration testing to interpret the HEAT sensor data.[12, 22]

At present, there are two main methods for interpreting the HEAT signals. The first (which we will call the isotherm criterion) assumes that during the heating pulse the HEAT sensor tracks the maximum depth that some fixed temperature (or isotherm) has progressed. The isotherm should correspond to the temperature at which the HEAT's Kapton tube chars enough to become electrically conductive. Thermo-gravimetric Analysis (TGA) of decomposing Kapton had originally indicated this was around 720 ^{o}C, but later arc jet tests indicated that the HEAT sensor correlated with an isotherm in the range of 750 - 900 ^{o}C (1023-1173 K).[9]

The second method of interpreting the HEAT sensor, the char criterion, comes from destructive post-test inspection of MISP tested in the arc jet. Over a range of conditions relevant to MSL, engineers observed that the final HEAT sensor depth (well after peak heating) consistently fell within the completely charred region of PICA at the top of a plug.[22] Using the calculated temperature and decomposition history, we can assess the flight HEAT data and the char and isotherm criteria. As before, we will examine simulation results for MISP1 and MISP2, and for each plug we use a TC driver using TC1.

Fig. 14 shows the results of these comparisons. As before, the TC depths are shown with the dashed lines. The boundaries of the char and virgin regions are denoted by green lines. The band of temperatures for the 750 - 900 ^{o}C range (1023-1173 K) is highlighted in red, while the reading of the HEAT sensor is shown with blue lines. The two lines of the HEAT represent the ± 0.7 mm depth uncertainty as specified in the MISP error budget. Based on the TC data and our simulations, we would expect the HEAT signal to roughly follow the red bars (~3 mm for MISP1, ~4 mm for MISP2) according to the isotherm criterion. The HEAT signal does not appear to follow any isotherm in this range, and we can estimate what temperature it is following when it crosses the thermocouple depths. This range is 590 – 640 K for TC1, and 450 – 480 K for TC2—much lower than observed in arc jet tests. Using the char criterion, we would also expect shallower final depths at the final time shown (t = 150 sec). In both plugs, the HEAT sensor depth traverses much further into the material than expected.

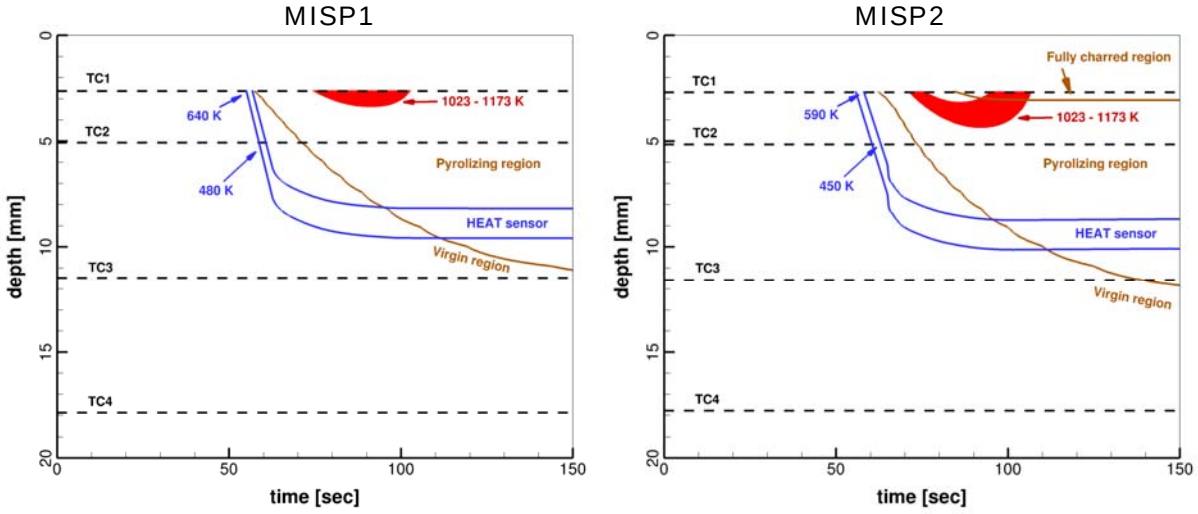

Fig. 14 HEAT sensor data at MISP1 and MISP2.

The disagreement using both the char and isotherm criterion demonstrates that the HEAT sensor performance in flight is considerably different from observed in arc jet test models. We are left to conclude that the flight data from the HEAT sensors is in disagreement with the thermocouples. Some explanation of the flight HEAT measurements may yet be found, perhaps due to differences in data acquisition systems between ground tests and flight. For now, the HEAT data will not be used for heatshield performance, and we instead rely on the TC data.

V. Bondline Temperature Response at MISP Locations

Of primary interest in heatshield performance is the bondline (the interface between the TPS and substructure) temperature response, and we can use the MISP flight TC data and in-depth modeling presented in Section IV to predict the bondline temperature response at each of the plug locations. The bondline temperature response is of

great interest to vehicle designers; the worst-case expected aerothermal environment guides the particular choice of TPS, and the bondline temperature determines the total thickness of that TPS. This limit is normally related to the adhesive at the attachment point or facesheet cure temperature. In the case of MSL, the design limit at the MISP locations was 523 K (250 °C).[2] Figure 15 shows the temperature response at the bottom of the MISP plug, based on a TC driver calculation. For each plug, we use the deepest thermocouple as it is closest to the bondline.

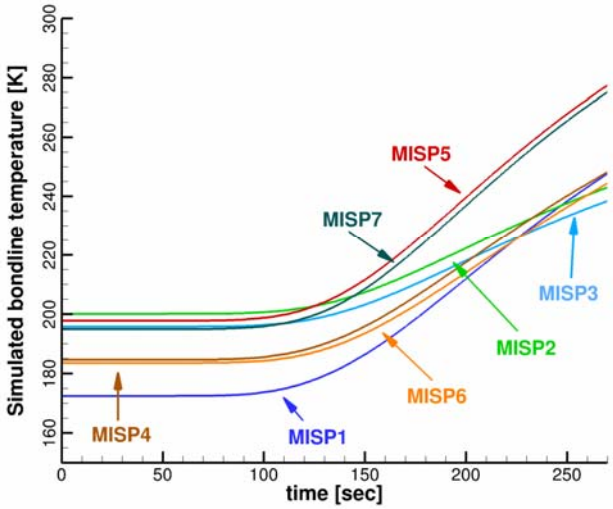

Fig. 15 FIAT Predicted bond-line temperature history at each MISP plug location.

Clearly, none of the plugs saw anywhere close to the design bondline temperature limit prior to heatshield ejection at 268 seconds. This was due to the conservative design of the MSL heatshield, including the aerothermal and material margins. These are the "nominal" results, in that these calculations of bondline temperature do not include any uncertainties due to material property variability.

The initial temperature (t = 0) will clearly influence the maximum temperature that is reached; MISP1 was initially the coldest and MISP2 the warmest. It is helpful to look at the rise in the temperature, and Table 8 lists both the maximum temperature and the rise in temperature. Here we see that MISP7 and MISP5 experienced the greatest rise in bondline temperature. This was due to the increased heating from turbulent flow, combined with a less dense substructure (as shown in Table 7) of MISP5 and MISP7 than other plugs that experienced turbulent heating (MISP2 and MISP3).

Table 8 Simulated bondline temperature response at the time of heatshield jettison

Plug	Peak $T_{bondline}$	$T_{bondline}$ Rise
	K	*K*
MISP1	247	75
MISP2	243	43
MISP3	238	43
MISP4	248	64
MISP5	277	80
MISP6	244	61
MISP7	275	80

In addition to estimating the bondline temperature, we perform a TPS sizing using the flight data and our design bondline temperature limit. We run a TC driver with a variable thickness of TPS—we pick the TPS thickness so that at 268 seconds the temperature reaches the bondline limit. To make our results more relevant to the acreage TPS sizing employed in design, we exclude the second and third material stack layers shown in Table 7 to be more representative of the acreage PICA. Those layers are for additional adhesive and PICA that are present only at the

MISP locations, and not part of the rest of the heatshield substructure. The resulting thickness is effectively an unmargined (or zero-margin) thickness calculation at the MISP locations.

In this sizing we impose the temperature boundary from TC2. This is necessary because in some plugs, TC3 and TC4 did not exceed our bondline temperature limit of 523 K. Table 9 shows the resulting thicknesses from the optimization for a bondline temperature limit of 523 K. According to our analysis, MISP3 would have required the least TPS, at 11.4 mm. At first, this is counter-intuitive, as this location was expected to see the highest peak heating—but MISP3 had a denser sub-structure than some of the other locations. MISP5 and MISP7 have had the greatest zero-margin TPS thickness, at 15.7 mm. As has been shown before, MISP5 and MISP7 experienced the highest integrated heat-load, with high laminar heating followed by turbulent transition and heating augmentation.[13, 22] The 15.7 mm represents the zero-margin thickness for the *as-flown* trajectory, based only on data at the MISP locations

To compare these thicknesses with the as-built thickness (31.8 mm) we must repeat the MSL margins process at the MISP locations. That will involve assessing the impact of design uncertainties and margins for trajectories, aerothermal heating, material variability and modeling, as well as manufacturing tolerances and other design considerations. With the MISP flight data now in hand, we conclude MSL could have landed safely with less heatshield mass, though the exact amount is the subject of ongoing work. Of course, heatshield designers must address many unknowns, particularly when working with challenging entry conditions, new mission concepts, and TPS materials. The successful landing of *Curiosity* and the data from MISP demonstrates that the MSL heatshield was conservatively designed and performed well.

Table 9 Unmargined TPS thickness for MSL as-flown trajectory

Plug	Thickness	Thickness
	mm	*in*
MISP1	14.6	0.57
MISP2	11.6	0.46
MISP3	11.4	0.45
MISP4	13.2	0.52
MISP5	15.7	0.62
MISP6	13.6	0.53
MISP7	15.7	0.62
Design	*31.8*	*1.25*

VI. Summary and Conclusions

The Mars Science Laboratory Entry Descent and Landing suite returned invaluable information regarding the aerothermal and heatshield performance during EDL. All the MISP TCs returned high quality signals, and the lack of drop-outs in the top thermocouples indicated that the TPS recession was probably less than 2.54 mm across the entire heatshield. The rapid change in near-surface TCs signaled a rapid progression of a turbulent transition front. The smooth-wall momentum thickness Reynolds number criterion ($Re_\theta > 200$) used in design was conservative—the heatshield experienced a combination of laminar and turbulent environments, and MSL was designed to withstand fully turbulent environments. The design would have still been conservative had MSL used the Re_θ criterion in such a way that environment predictions switched from laminar to turbulent as soon as any location on the heatshield exceeded Re_θ of 200. Despite this, the Re_θ did not predict the rapid progression of turbulent transition.

The roughness Reynolds number, Re_{kk}, appeared to be a better indicator of transition time and transition front speed. Using CFD on the BET along with existing roughness induced transition criteria, we assessed the possible roughness heights and compared to the observed transition timing in flight. These roughness heights were derived from ground testing, and ranged from small-scale PICA distributed roughness, to larger heights from the instrumentation plugs and gaps between the PICA tiles. We believe it is likely that a series of roughness heights of the scale of the PICA gap fillers and MISP plugs acted as a distributed roughness—such a scenario seems to correlate well with existing transition data. However, additional ballistic range and roughness studies may improve our understanding of turbulent transition due to distributed roughness in CO_2, and an in-situ investigation of the MSL heatshield by *Curiosity* could answer question on what types of roughness developed during entry. In future

missions, it may be help to try to reduce the roughness element disturbances on the heatshield and instrumentation; indeed, MISPs tested without RTV sealing around the edge do not develop roughness elements in arc jet tests.

For the TPS performance, we are able to predict in-depth performance using a TC driver approach combined with the actual flight data. The TC driver analysis shows that below the top thermocouple material temperatures are well-predicted with the PICA thermal model. Even when shallowest TC response is used to estimate the deepest TC, the model is generally over-predictive at the peak values. The current model is well within ±50 K at all times for the deep and shallow TCs. This gives us increased confidence for designing potentially thinner (and lighter) PICA heatshields for future Mars missions. We observed that in the plugs, the bottom two thermocouples remained in virgin PICA for the majority of the entry, while the top two thermocouples were in pyrolyzing and charring regions. Additional publications from MEDLI on PICA thermal property characterization are expected to follow; combined with the flight data and inverse analysis we may further improve material models and the techniques used to develop the models.

While the TC data have been useful in reconstructing both the aerothermal environment and the ablator response, there remain unresolved issues with the HEAT sensors. The HEAT-reported depths from flight do not appear to agree with the correlations developed from ground tests. The HEAT data are inconsistent with both the char and isotherm criteria, and the HEATs reported much greater depths sooner than suggested by thermocouples and material simulations. Until a reasonable explanation for the HEAT performance is possible, we do not expect to use the data in further MSL heatshield reconstruction work.

Finally, we used the MISP thermocouple data to estimate the flight bondline temperature rise, and also to perform zero-margin sizing of the TPS based on the as-flown trajectory. Surprisingly, MISP7 probably experienced the greatest temperature increase at the bondline, due to both to the substructure at that plug and turbulent heating. A zero-margin re-sizing of the PICA heatshield at the MISP7 location resulted in 15.7 mm. Future work will focus on the margin design process of MSL using the MEDLI data and associated analysis, to improve the TPS sizing and margins policy for future Mars missions.

Acknowledgments

Portions of this work were completed under contract NNA10DE12C to ERC Inc., NNA09DB39C to Jacobs Technology Inc., and NASA grant NNX12AF94A from the NRA Research Opportunities in Aeronautics 2012. The authors are grateful to Mike Wilder and Dan Reda for their PICA roughness measurements and discussions on roughness-induced transition. The authors also thank Erika Rodriguez, Karl Edquist, Robin Beck and David Saunders for their time and helpful feedback.

References

[1] Steltzner, A., et al, "Mars Science Laboratory Entry, Descent and Landing System Overview," AIAA 2013-236, *AAS/AIAA Spaceflight Mechanics Meeting*, Kauai, Hawaii, February 2013.

[2] Wright, M., Beck, R., Edquist, K., Driver, D., Sepka, S., Slimko, E., Willcockson, W., DeCaro, A., and Hwang, H., "Sizing and Margins Assessment of the Mars Science Laboratory Aeroshell Thermal Protection System," *41st AIAA Thermophysics Conference*, AIAA 2009-4231, San Antonio, Texas, June 2009.

[3] Beck, R., Driver, D., Wright, M., Laub, B., Hwang, H., Slimko, E., Edquist, K., Sepka, S., Willcockson, W., and Thames, T., "Development of the Mars Science Laboratory Heatshield Thermal Protection System," *41st AIAA Thermophysics Conference*, AIAA 2009-4229, San Antonio, Texas, June 2009.

[4] Edquist, K. T., Dyakonov, A. A., Wright, M. J., and Tang, C.-Y., "Aerothermodynamic Design of the Mars Science Laboratory Heatshield," AIAA 2009-4075, *AIAA Thermophysics Conference*, San Antonio, Texas, June 2009.

[5] Tran, H., Johnson, C. E., Rasky, D. J., Hui, F. C., Hsu, M.-T., Chen, T., Chen, Y.-K., Paragas, D., and Kobayashi, L., "Phenolic Impregnated Carbon Ablators (PICA) as Thermal Protection Systems for Discovery Missions," NASA TM-110440, April 1997.

[6] Gazarik, M., Wright, M., Little, A., Cheatwood, F. M., Herath, J., Munk, M., Novak, F., and Martinez, E., "Overview of the MEDLI Project," IEEE Paper 2008-1510, *IEEE Aerospace Conference*, Big Sky, Montana, March 2008.

[7] Little, A., et al, "The Mars Science Laboratory (MSL) Entry, Descent And Landing Instrumentation (MEDLI): Hardware Performance and Data Reconstruction," AAS 13-078, *AAS Guidance and Navigation Conference*, Breckenridge, Colorado, February 2013.

[8] Karlgaard, C., Kutty, P., Schoenenberger, M., Shidner, J., Munk, M., "Mars Entry Atmospheric Data System Trajectory Reconstruction Algorithms and Flight Results," AIAA 2013-0028, *AIAA Aerospace Sciences Meeting*, Grapevine, Texas, January 2013.

[9] Bose, D., White, T., Santos, J., Feldman, J., Mahzari, M., Olson, M., and Laub, B., "Initial Assessment of Mars Science Laboratory Heatshield Instrumentation and Flight Data," AIAA 2013-908, *AIAA Aerospace Sciences Meeting*, Grapevine, Texas, January 2013.

[10] ASTM Standard E377-08, "Standard Practice for Internal Temperature Measurements in Low-Conductivity Materials," ASTM International, West Conshohocken, PA, 2008, DOI: 10.1520/E0377-08, www.astm.org.
[11] Bose, D., White, T., Santos, J., Feldman, J., Mahzari, M., and Edquist, K., "A Reconstruction of Aerothermal Environment and Thermal Protection System Response of the Mars Science Laboratory Entry Vehicle," AAS 13-311, *AAS/AIAA Spaceflight Mechanics Meeting,* Kauai, Hawaii, February 2013.
[12] Santos, J., Jacobs, T., and Martinez, E., "Isotherm Sensor Calibration Program for Mars Science Laboratory Heat Shield Flight Data Analysis," *42nd AIAA Thermophysics Conference*, AIAA 2011-3955, Honolulu, Hawaii, June 2011.
[13] Milos, F., Chen, Y., Squire, T. "Analysis of Galileo Probe Heatshield Ablation and Temperature Data," *Journal of Spacecraft and Rockets*, Vol. 36, No. 3, 1999, pp. 298-306.
[14] Mahzari, M., Braun, R., White, T., and Bose, D., "Preliminary Analysis of the Mars Science Laboratory's Entry Aerothermodynamic Environment and Thermal Protection System Performance," *51st AIAA Aerospace Sciences Meeting*, AIAA 2013-0185, Grapevine, Texas, January 2013.
[15] Mahzari, M., Braun, R., and White, T., "Reconstruction of Mars Pathfinder Aerothermal Heating and Heatshield Material Response Using Inverse Methods," *43rd AIAA Thermophysics Conference*, AIAA 2012 2872, New Orleans, Louisiana, June 2012.
[16] Edquist, K., Hollis, B., Bose, D., White, T., and Mahzari, M., "Reconstruction of the Mars Science Laboratory Heatshield Aerothermodynamics," AIAA 2013-2781 *44th AIAA Thermophysics Conference*, San Diego, California, June 2013.
[17] Wright, M. J., Candler, G. V., and Bose, D., "Data-Parallel Line Relaxation Method for the Navier-Stokes Equations," *AIAA Journal*, Vol. 36, No. 9, 1998, pp. 1603-1609.
[18] Karlgaard, C., Schoenenberger, M., Kutty, P., and Shidner, J., "Mars Science Laboratory Entry, Descent, and Landing Trajectory and Atmosphere Reconstruction," AAS 13-307, *AAS/AIAA Space Flight Mechanics Meeting*, Kauai, Hawaii, February 2013.
[19] Mitcheltree, R. and Gnoffo, P. "Wake Flow About a MESUR Mars Entry Vehicle," AIAA 94-1958, *31st AIAA Thermophysics Conference*, Colorado Springs, Colorado, June 1994.
[20] Reda, D. C., Wilder, M. C., Bogdanoff, D. W., and Prabhu, D. K., "Transition Experiments on Blunt Bodies with Distributed Roughness in Hypersonic Free Flight," *Journal of Spacecraft and Rockets*, Vol. 45, No. 2, March–April 2008, pp. 210–215.
[21] Reda, D. C., Wilder, M. C., and Prabhu, D. K., "Transition Experiments on Blunt Bodies with Isolated Roughness Elements in Hypersonic Free Flight," *Journal of Spacecraft and Rockets*, Vol. 47, No. 5, September–October 2010, pp. 828–835.
[22] Bose, D., "Mars Science Laboratory Heat Shield Instrumentation and Post-Flight Analyses," AIAA 2013-2778, *AIAA Thermophysics Conference*, San Diego, California, June 2013.
[23] Tang, C., Edquist, K. T., Wright, M. J., Sepka, S., and Cassel, A., "Numerical Simulations of Protruding Gap Fillers on the Mars Science Laboratory Heatshield," AIAA 2009-4077, *AIAA Thermophysics Conference*, San Antonio, Texas, June 2009.
[24] Szalai, C., Thoma, B., Lee, W., Maki, J., Willcockson, W., Venketapathy, R., and White, T. "Mars Exploration Rover Heatshield Observation Campaign," AIAA 2011-3956, *AIAA Thermophysics Conference*, Honolulu, Hawaii, June 2011.
[25] Mahzari, M., White, T., Braun, R., and Bose, D., "Inverse Estimation of Mars Science Laboratory's Entry Aerothermal Environment and Thermal Protection System Response," AIAA 2013-2780, *43rd AIAA Thermophysics Conference*, San Diego, California, June 2013.
[26] Chen, Y. and Milos, F., "Ablation and Thermal Response Program for Spacecraft Heatshield Analysis," *Journal of Spacecraft and Rockets*, Vol. 36, No. 3, 1999, pp. 475-483.
[27] F.S. Milos and Y.K. Chen, "Ablation and Thermal Response Property Model Validation for Phenolic Impregnated Carbon Ablator," *Journal of Spacecraft and Rockets*, Vol. 47, No. 5, 2010, pp. 786-805.